Quantum Design for Advanced Qubits

Feng-Ming Liu[1,2,3], Ming-Cheng Chen[1,2,3], Can Wang[1,2,3], Shao-Wei Li[1,2,3], Zhong-Xia Shang[1,2,3], Chong Ying[1,2,3], Jian-Wen Wang[1,2,3], Cheng-Zhi Peng[1,2,3], Xiaobo Zhu[1,2,3], Chao-Yang Lu[1,2,3], Jian-Wei Pan[1,2,3]

[1]Hefei National Laboratory for Physical Sciences at Microscale and Department of Modern Physics, University of Science and Technology of China, Hefei, Anhui 230026, China [2]Shanghai Branch, CAS Centre for Excellence and Synergetic Innovation Centre in Quantum Information and Quantum Physics, University of Science and Technology of China, Shanghai 201315, China [3]Shanghai Research Center for Quantum Sciences, Shanghai 201315, China

The increasingly complex quantum electronic circuits with a number of coupled quantum degrees of freedom will become intractable to be simulated on classical computers, and requires quantum computers for an efficient simulation. In turn, it will be a central concept in quantum-aided design for next-generation quantum processors. Here, we implement variational quantum eigensolvers to simulate a Josephson-junction-array quantum circuit, which leads to the discovery of a new type of high-performance qubit, "plasmonium". We fabricate this new qubit and demonstrate that it exhibits not only a high single- and two-qubit gate fidelity, but also a shrinking physical size and larger anharmonicity than the transmon, which will offer a number of advantages for scaling up multi-qubit devices. Our work opens the way to designing advanced quantum processors using existing quantum computing resources.

Main text

The past half century has witnessed the rapid development of integrated circuits from several to billions of electronic components. A key enabling method was the electronic computer-aided design software, with which the engineers used the existing computers to calculate and simulate increasingly more complex electronic circuits, to inspire and

design next-generation higher-performance processors. Similarly, efficient simulations of quantum hardware will play an important role in designing large-scale quantum computers[1-5].

To improve the performance of superconducting quantum computing, a combination of different efforts are undertaken: (1) reducing the noise from materials and environment; (2) designing new, higher-performance qubits with physical protection from the noise; (3) actively correcting the error during quantum computing by quantum error correction. In particular, designing a hardware-efficient logical qubit, i.e. noise-protected physical qubit, will be a shortcut to implement fault-tolerant quantum computing by reducing the resource overhead in quantum error correction.

The past decades have witnessed a continuous improvement of the performance of the superconducting qubits. In principle, noise-protected qubits can be realized in quantum electronic circuit level by elaborately coupling many quantum degrees of freedom to achieve robust quantum states[6]. A large number of coupled quantum degrees of freedom is the key to construct ultra-low-noise qubits. While the calculations of quantum circuits could be done classically on a small scale, it is expected that the resources required for the classical simulations grow exponentially $O(d^N)$ with N coupled d-dimensional quantum degrees of freedom. Therefore, it is important to exploit the simulation capability of intermediate-scale quantum computers—for instance, those before full-fledged for prime factoring—to effectively aid the design of future higher-performance quantum computers (Fig. 1a).

In this work, we demonstrate quantum-aided design based on variational quantum simulation[7-10] of a superconducting electronic circuit model to design a new high-performance qubit. The discovered new qubit has a remarkable feature superior to the widely used transmons and is fully compatible with the control technologies as in the transmon. This advanced qubit breaks a trade-off in transmon between charge noise sensitivity and qubit anharmonicity[5,11] and can bring key advantages, including a shrinking physical size, reducing state leakage[12], and alleviating frequency crowding

problem[13] in multi-qubit devices.

We start from the variational quantum simulation of the energy spectrum for the superconducting electronic circuit model (Fig. 1b), which provides the crucial property to identify the new qubit. The circuit has a shunted Josephson junction array as inductance, which adds more complexity to the device but at the same time provide more design flexibility[14]. The single Josephson junction in this system is parametrized by its Josephson energy E_J, while the capacitance and inductance can be parametrized by the capacitance and inductance C and L, or equivalently by $E_C = e^2/2C$ and $E_L = (\hbar/2e)^2/L$, which is the charging and inductive energy, respectively. The Hamiltonian of this circuit can be written as[15]

$$H = -4E_C\hat{n}^2 - E_J\cos(\hat{\phi} + \phi_{ext}) + \frac{1}{2}E_L\hat{\phi}^2 \tag{1}$$

where ϕ is the phase across the inductance, and n is the number of cooper pairs tunneled between the two islands of the circuit which is conjugate to ϕ. ϕ_{ext} is the external flux threading through the loop between the Josephson junction and inductance, in unit of the reduced superconducting flux quantum $\Phi_0/2\pi = \hbar/2e$. As the quantum variables n and ϕ are both continuous, we will use the Fock-state basis of its harmonic part $H_{har} = -4E_C\hat{n}^2 + \frac{1}{2}E_L\hat{\phi}^2$ to discretely encode the system Hamiltonian. Let a and $a^\dagger$ be the annihilation and creation operator, the whole circuit Hamiltonian becomes

$$H = \omega\hat{a}^\dagger\hat{a} - E_J\cdot\frac{\hat{D}(iA)e^{i\phi_{ext}} + \hat{D}(-iA)e^{-i\phi_{ext}}}{2} \tag{2}$$

where $\omega = \sqrt{8E_CE_L}$ is the transition frequency of H_{har}, $A = (2E_C/E_L)^{1/4}$, and $\hat{D}$ is the displacement operator defined as $\hat{D}(\alpha) = \exp(\alpha\hat{a}^\dagger - \alpha^*\hat{a})$. We truncate the Hilbert space to finite dimensions so that it can be mapped to the computational basis of our quantum processor. Here, we keep the Fock states up to 7 photons (Fig. 2a),

which has enough accuracy for our quantum simulation.

The variational quantum circuit is shown in Fig. 2b. The role of this circuit is to implement unitary rotation from the computational bases (Fock states) to the energy eigenstates. The circuit consists of two 2-qubit and two 3-qubit $\sqrt{iSWAP}$ gates (see SI) with embedding variational single-qubit gates on both sides of them. In this work, we utilized the subspace-search VQE algorithm to find the lowest three energy eigenstates simultaneously[16]. We initialize the quantum state in the lowest three Fock states and then execute the same unitary quantum circuit. As the input states are orthogonal, the final states after the circuit are also orthogonal. Therefore, by measuring the expectation value of Hamiltonian (Fig. 2c), we obtain the expected energies of the three orthogonal states, which are labelled E_0, E_1 and E_2. We define the cost function for variational optimization of the quantum circuit as

$$F_{\text{cost}} = 5 \times E_0 + 4 \times E_1 + 2 \times E_2 ,$$

where the weighing coefficients for lower eigenstates are larger than higher eigenstates. Thus, when the cost function is optimized to its global minima, the three output orthogonal states will be the three lowest eigenstates automatically.

In our algorithmic experiment, the design parameter E_L, the inductive energy of the Josephson junction array, is swept from 0.2 GHz to 3 GHz while the other parameters are fixed at $E_C = 0.7$ GHz, $E_J = 4.5$ GHz and $\phi_{ext} = \pi / 2$. Figure 2d shows the cost function and the corresponding energies of the three orthogonal states (the inset figure) as a function of the number of iterations in a typical example of the optimization process at $E_L = 3.0$ GHz. The cost function is optimized by the simultaneous perturbation stochastic approximation method[17]. We observe a competition phenomenon in the energies during the optimization: the energies of 1st and 2nd excited states first decrease and then increase to the steady values, while the cost function decreases gradually. After completely sweeping the design parameter E_L, we plot the energy spectrum of the

three lowest eigenstates as a function of E_L in the Fig. 2e. We see that the results agree well with the ideal values and interestingly, the excited states have smaller average deviated energies (~0.52 GHz) than the ground state (~0.76 GHz). The reason is that, in contrast to the excited states, the quantum state error in the ground state can only increase the energy. These energy deviations are partly contributed from the white noise through the circuit decoherence, which can be reduced by quantum error mitigation method (see SI). The results before and after error mitigation are represented by circles and crosses in Fig. 2e, respectively. We see that the average deviations of energy estimation have reduced by 67%.

In the energy spectrum, we observe an anti-crossing signal between the two excited states when the inductive energy E_L is ~ 0.45 GHz, which indicates the presence of a phase transition. The phase transition is originated from the multiple valley profile of the potential in the system Hamiltonian. The physical picture is shown in Fig. 3a and 3b. Before the transition, the potential has two lowest valleys located around phase 0 and 2π (Fig. 3a for $E_L = 0.2$ GHz) and the eigenstates $|0\rangle$ and $|1\rangle$ localized in different valleys. As the parameter E_L increases, all of the potential valleys together with the eigenstates localized in them are lifted up. When the energies of excited eigenstates $|1\rangle$ and $|2\rangle$ in different valleys become closer, there exists an anti-crossing in energy spectrum. When the parameter E_L further increases, there will be only one potential valley left in phase space, and the lowest two energy states are both located in this single valley (Fig. 3b for $E_L = 2.0$ GHz). In fact, the parameter regime corresponding to the left side of the anti-crossing is the so-called heavy Fluxonium[18]. Because of the small overlap of the wavefunctions for computational bases in different valleys, this type of qubit possesses large relaxation time up to 8 ms. However, the regime corresponding to the right side of the anti-crossing is never studied in previous works. In the followings, we will detailly discuss the qubit operated in this regime.

The potential profile of our new qubit resembles the transmon qubit but extends from

$[-\pi,\pi)$ to the whole phase space. We call this new qubit Plasmonium, because the qubit is driven by plasmon transition in single phase valley, which is in contrast to Fluxonium qubits using fluxon transition between two different phase valleys.

In Plasmonium qubit, with the help of a shunted inductance, the charge degree of freedom becomes a continuous variable and the charge bias noise can be fully eliminated through a gauge transformation. In this way, the tradeoff between anharmonicity and charge noise sensitivity in Transmon qubit are completely avoided. Thus, we are able to use a small shunt capacitance to increase the anharmonicity and reduce the device footprint without the influence of charge noise.

Except the elimination of charge noise, our Plasmonium qubits keep high coherence time T_2 in a large tunable band of transition frequency. We compare the flux sensitivity of Plasmonium with transmon and two other variants of the inductively shunted Josephson junction model, heavy Fluxonium and Quarton[19]. Their energy dispersion $\partial f_{01} / \partial \phi_{ext}$ with external flux versus the transition frequency detuning from their first-order flux insensitive point is plotted in Fig. 3c (see SI). We observe that the flux sensitivity is of Plasmonium is much less than heavy Fluxonium and Quarton when detuned the same level from its flux-insensitive point. It is also less than the Transmon qubit with symmetric junctions. This is because the Plasmonium can be viewed as a Transmon with a non-symmetric composite junction, including a single junction and a junction array, to reduce the flux sensitivity. Therefore, when neglecting the other decoherence channel which is usually small compared with flux noise, the Plasmonium qubit has the largest high-T_2 frequency band[20].

Next, we move to the experimental test of the new qubits. In Fig. 4a, we show the scanning electron microscopy (SEM) image of the fabricated Plasmonium qubits, which has qubit length of $240\ \mu\text{m}$, only 40% of a typical transmon. The key element, the inductance of $E_L = 2.20$ GHz, is implemented by 37 large-area Al/Al oxide/Al Josephson junctions connected in series[21,22]. In our samples, we keep the structure of

Plasmonium to like Transmon to the most extent, where the qubit's frequency is tuned by an inductively coupled transmission line (TL), the qubit's transition is driven by another capacitively coupled TL, and the qubit is measured by probing a dispersively coupled resonator through a readout TL (Fig. 4a). Therefore, our qubits have a good compatibility with Transmon's operating system, which is widely used in contemporary quantum computing experiments.

The large anharmonicity of the Plasmonium qubit is confirmed by its energy spectrum as shown in Fig. 4b. We first apply an X gate to initialize the qubit in $|1\rangle$ state, and then tune the external flux threading the Josephson loop to different bias points where microwave pulses with varying frequencies are applied to probe the transition frequencies f_{01} and f_{12}. From the resulting energy spectrum, we extract the qubit parameters to be $E_C = 0.60$ GHz, $E_J = 5.61$ GHz and $E_L = 2.20$ GHz, agreeing well with our design. From the data, we see the anharmonicity has a minimum 490 MHz at the flux insensitive point, which is about 50% larger than the typical Transmons and can reduce the state leakage error by 55%. We note that this anharmonicity is not the upper bound of Plasmonium because it can be further increased by reducing the capacitance of the qubit. The Plasmonium qubit also exhibits high coherence time. At its flux insensitive point, we measured its relaxation time $T_1 = 32.5 \pm 1.2$ μs and dephasing time $T_2 = 16.3 \pm 0.9$ μs through Ramsey interferometry (Fig. 4d). This result is slightly better than the best transmon qubit fabricated on the same chip. In Fig. 4c, we present the measured coherence time at different flux detuning. The result shows that the new qubit still keeps the dephasing time above 2 μs when detuning from flux insensitive point as much as 400 MHz, which demonstrates a large high-T_2 frequency band.

In order to characterize the quantum gate performance of the new qubit, we further capacitively coupled two Plasmonium qubits via a frequency-tunable coupler. The performance of simultaneous single-qubit gates and two-qubit iSWAP-like gates are

characterized by cross-entropy benchmarking (XEB)[23,24]. In these quantum gate operations, the larger anharmonicity of Plasmonium can lead to larger drive amplitude of single-qubit gates and coupling strength in two-qubit gates because of the reduced leakage error. As a result, we obtained the average fidelity of simultaneous single qubit gates to be 99.85(1)% and 99.86(1)% and two-qubit iSWAP-like gate to be 99.58(3)%. We note that this is the first batch of the new qubit device we fabricated but, nonetheless, these measured fidelities of universal gate set have exceeded the transmons used in the quantum design. In the future work, we can make use of established technology in the transmon qubit to optimize the Plasmonium and use it to construct multi-qubit devices. For example, with recent progress in new superconducting materials and surface treatment method[25-27], we expect that the lifetime and coherence time of Plasmonium qubits can be improved to several hundreds of microseconds.

In summary, we have proposed and demonstrated the concept of quantum-aided design to discover a new advanced superconducting qubit, the Plasmonium, with superior features than the transmon. Though the scale of the present quantum design can be simulated on classical computers, our work demonstrate a promising route to use intermediate-scale quantum simulators beyond the classical simulation capacity to design hardware efficient noise-protected qubits to reduce the resource overhead of fault-tolerant quantum computing.

References and notes

1. Devoret, M. H. & Schoelkopf, R. J. Superconducting Circuits for Quantum Information: An Outlook. *Science* **339**, 1169–1174 (2013).
2. Mooij, J. E. Josephson Persistent-Current Qubit. *Science* **285**, 1036–1039 (1999).
3. You, J. Q., Hu, X., Ashhab, S. & Nori, F. Low-decoherence flux qubit. *Phys. Rev. B* **75**, 140515 (2007).
4. Yan, F. et al. The flux qubit revisited to enhance coherence and reproducibility. *Nat Commun* **7**, 12964 (2016).

5. Koch, J. *et al.* Charge-insensitive qubit design derived from the Cooper pair box. *Phys. Rev. A* **76**, 042319 (2007).
6. Kapit E. Hardware-efficient and fully autonomous quantum error correction in superconducting circuits. *Phys. Rev. Lett*. **116**, 150501 (2016).
7. Hempel, C. et al. Quantum Chemistry Calculations on a Trapped-Ion Quantum Simulator. *Phys. Rev. X* **8**, 031022 (2018).
8. Google AI Quantum and Collaborators et al. Hartree-Fock on a superconducting qubit quantum computer. *Science* **369**, 1084–1089 (2020).
9. Kandala, A. et al. Hardware-efficient variational quantum eigensolver for small molecules and quantum magnets. *Nature* **549**, 242–246 (2017).
10. Kyaw, T. H. et al. Quantum computer-aided design: digital quantum simulation of quantum processors. *arXiv:2006.03070* (2020).
11. Schreier, J. A. et al. Suppressing charge noise decoherence in superconducting charge qubits. *Phys. Rev. B* **77**, 180502 (2008).
12. Chen, Z. et al. Measuring and Suppressing Quantum State Leakage in a Superconducting Qubit. *Phys. Rev. Lett*. **116**, 020501 (2016).
13. Hertzberg, J. B. et al. Laser-annealing Josephson junctions for yielding scaled-up superconducting quantum processors. *npj Quantum Inf* **7**, 129 (2021).
14. Hafezi, M., Adhikari, P. & Taylor, J. M. Engineering three-body interaction and Pfaffian states in circuit QED systems. *Phys. Rev. B* **90**, 060503 (2014).
15. Manucharyan, V. E., Koch, J., Glazman, L. I. & Devoret, M. H. Fluxonium: Single Cooper-Pair Circuit Free of Charge Offsets. *Science* **326**, 113–116 (2009).
16. Nakanishi, K. M., Mitarai, K. & Fujii, K. Subspace-search variational quantum eigensolver for excited states. *Phys. Rev. Research* **1**, 033062 (2019).
17. Spall, J. C. Multivariate stochastic approximation using a simultaneous perturbation gradient approximation. *IEEE Trans. Automat. Contr.* **37**, 332–341 (1992).
18. Earnest, N. et al. Realization of a Λ System with Metastable States of a Capacitively Shunted Fluxonium. *Phys. Rev. Lett.* **120**, 150504 (2018).

19. Yan, F. et al. Engineering Framework for Optimizing Superconducting Qubit Designs. *arXiv:2006.04130* (2020).
20. Sank, D. et al. Flux Noise Probed with Real Time Qubit Tomography in a Josephson Phase Qubit. *Phys. Rev. Lett.* **109**, 067001 (2012).
21. Masluk, N. A., Pop, I. M., Kamal, A., Minev, Z. K. & Devoret, M. H. Microwave Characterization of Josephson Junction Arrays: Implementing a Low Loss Superinductance. *Phys. Rev. Lett.* **109**, 137002 (2012).
22. Nguyen, D. V. & Basko, D. M. Inhomogeneous Josephson junction chains: a superconducting meta-material for superinductance optimization. *Eur. Phys. J. Spec. Top.* **226**, 1499–1514 (2017).
23. Bouland, A., Fefferman, B., Nirkhe, C. & Vazirani, U. On the complexity and verification of quantum random circuit sampling. *Nature Phys* **15**, 159–163 (2019).
24. Boixo, S. et al. Characterizing quantum supremacy in near-term devices. *Nature Phys* **14**, 595–600 (2018).
25. Place, A. P. M. et al. New material platform for superconducting transmon qubits with coherence times exceeding 0.3 milliseconds. *Nat Commun* **12**, 1779 (2021).
26. Osman, A. et al. Simplified Josephson-junction fabrication process for reproducibly high-performance superconducting qubits. *Appl. Phys. Lett.* **118**, 064002 (2021).
27. Mergenthaler, M. et al. Ultrahigh Vacuum Packaging and Surface Cleaning for Quantum Devices. *Review of Scientific Instruments* **92**, 025121 (2021).

Figure Captions

Fig. 1| The concept of quantum design. (a) Quantum design uses the existing quantum computing resource to accelerate the development of next-generation quantum computers. It plays the same role of electronic computer-aided design for classical computers, which has great achievements in the past decades. **(b)** The outline of our work. We used a variational quantum eigensolver to simulate a superconducting quantum electronic circuit. The circuit model has a Josephson junction array as a

shunted inductance. We fabricated and tested the new qubit guiding by the quantum simulation result and obtain an advanced qubit with better performance than the transmon. We named the new qubit as Plasmonium.

Fig. 2| Variational quantum simulation. (a) Fock states up to 7 photons used as the bases to encode the system Hamiltonian. **(b)** The variational quantum circuit used to rotate the Fock states to the eigenstates. It has 26 variational parameters in the embedded single-qubit gates. The cost function is defined as a weighting sum of the three lowest energy eigenvalues: E_0, E_1 and E_2. **(c)** The system Hamiltonian shown in the Fock bases. It is mapped to a weighting sum of Pauli operators (20 terms) through Gray code to estimate the energy eigenvalues. **(d)** A typical optimization process for design parameter $E_L = 3.0$ GHz. The inset shows the three lowest energy eigenvalues as a function of the number of iterations. **(e)** The energy spectrum of the three lowest eigenvalues as a function of the parameter E_L. The error-mitigated values are also shown.

Fig. 3| Characteristics of the new qubit. (a)(b) Potential profile of the system Hamiltonian and the corresponding energy eigenvalues before ($E_L = 0.2$ GHz) and after ($E_L = 2.0$ GHz) the phase transition, respectively. **(c)** Flux noise sensitivity as a function of the detuning from the flux insensitive point. Four types of qubits are put into comparison: Transmon, Heavy Fluxonium , Quarton and Plasmonium.

Fig. 4| Fabrication and test of the new qubit. (a) The SEM images of the Plasmonium qubit. The geometry layout of the new qubit is similar to the transmon qubit. The zoom-in shows the inductively shunted Josephson junction array. **(b)** The transition spectrum of the Plasmonium qubit as a function of the external flux. The $|0\rangle \leftrightarrow |1\rangle$ and $|1\rangle \leftrightarrow |2\rangle$ transitions are theoretically fitted by the green and red solid lines respectively.

The additional gray dotted line is due to the non-ideal input of microwave driving signal. **(c)** The dephasing time as a function of the detuning from its flux insensitive point. **(d)** The energy relaxation time and the dephasing time measurement at the flux insensitive point. **(e)** The cross entropy benchmarking of single and two-qubit gates. A single cycle in single-qubit gate benchmarking includes a single qubit gate of Q1 and Q2 respectively and a single cycle in two-qubit gate benchmarking includes a layer of single-qubit gate and a layer of two-qubit gate. The duration of a single-qubit gate and a two-qubit gate are 20ns and 10ns, respectively.

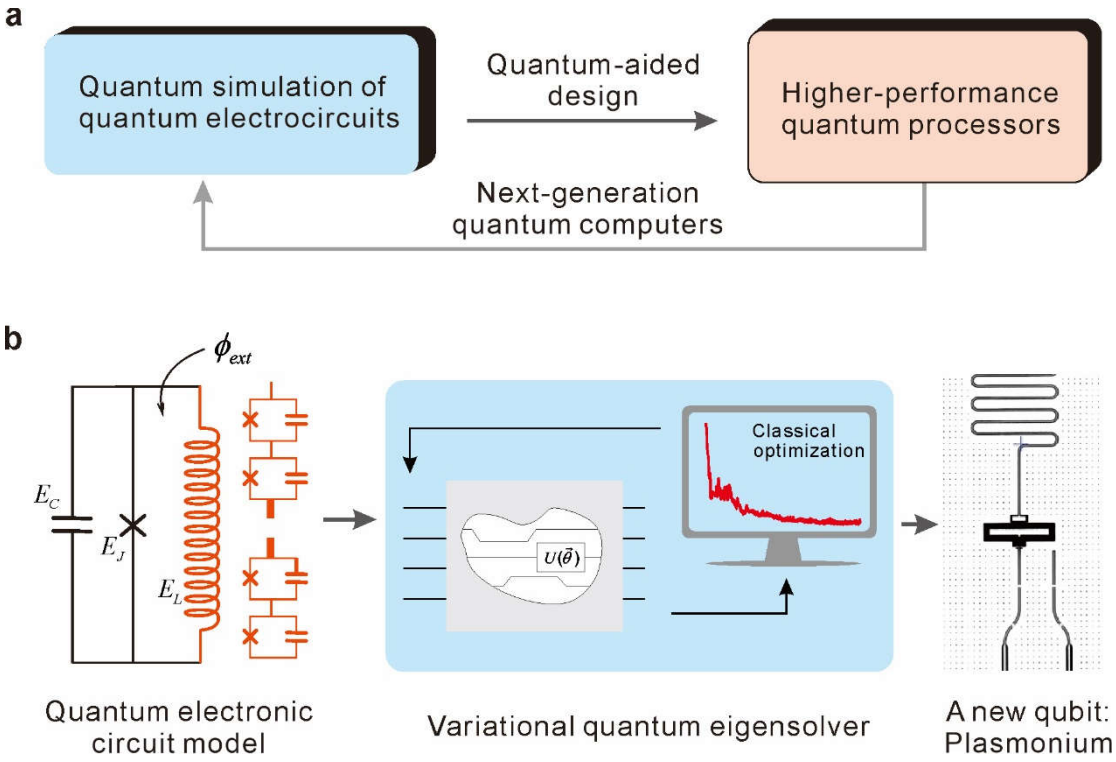

Figure 1

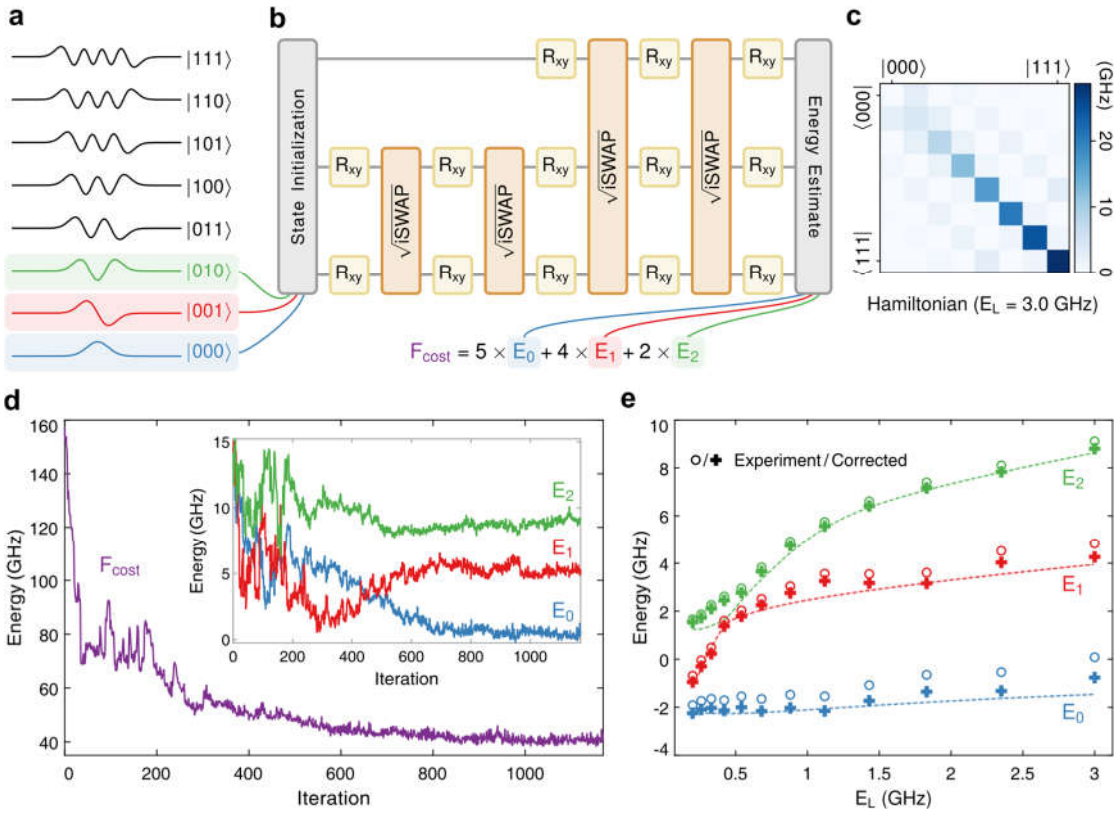

Figure 2

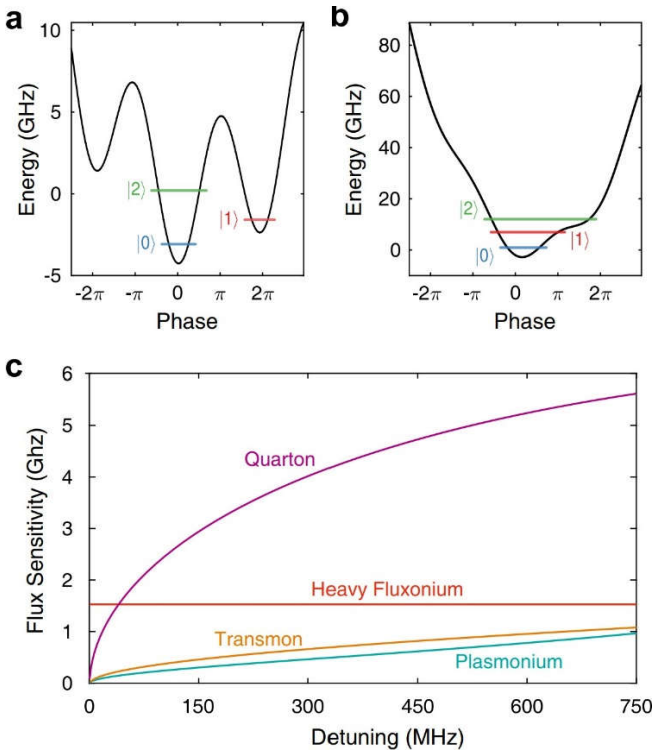

Figure 3

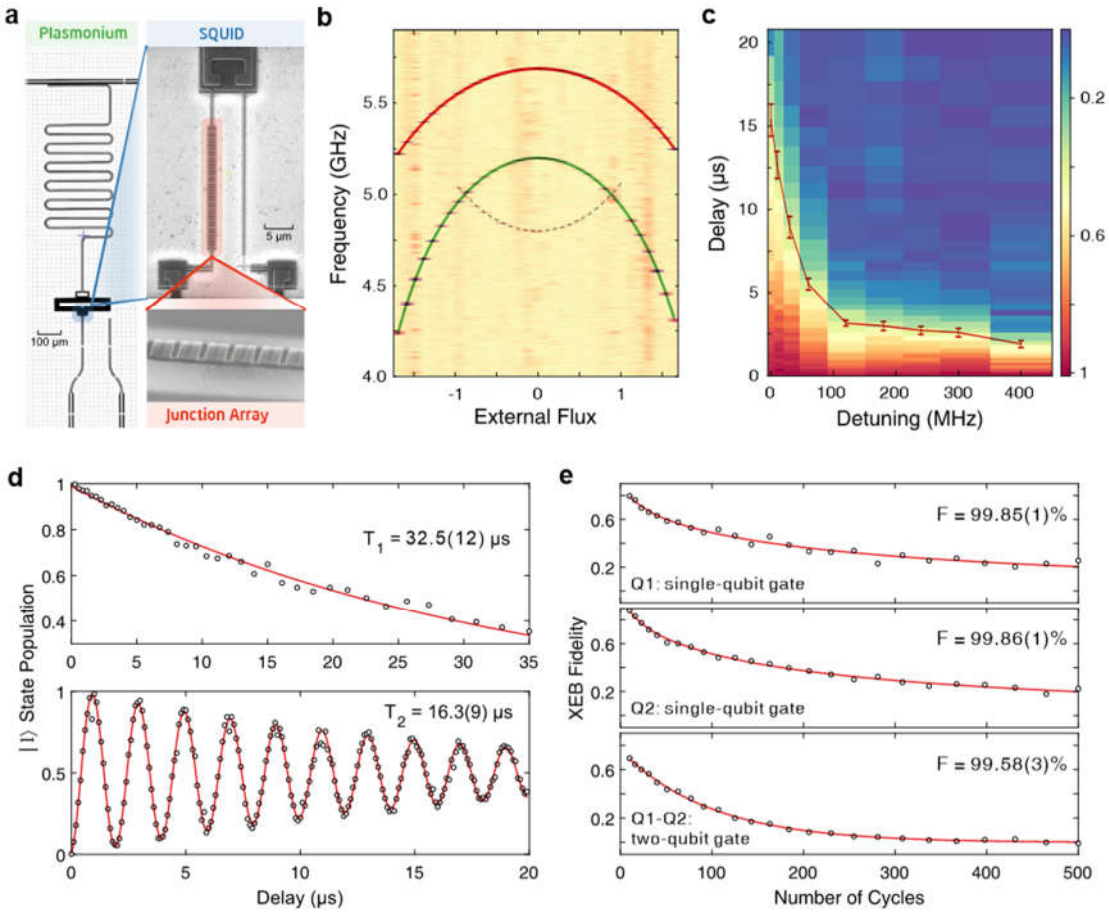

Figure 4